IEEE Access
Multidisciplinary | Rapid Review | Open Access Journal

Received February 17, 2020, accepted March 2, 2020, date of publication March 5, 2020, date of current version March 18, 2020.

Digital Object Identifier 10.1109/ACCESS.2020.2978789

A Secured Energy Management Architecture for Smart Hybrid Microgrids Considering PEM-Fuel Cell and Electric Vehicles

XUAN GONG[1], FEIFEI DONG[2], MOHAMED A. MOHAMED[3,4], (Member, IEEE), OMER M. ABDALLA[5,6], AND ZIAD M. ALI[5,7]

[1]School of Electrical Engineering and Automation, Anhui University, Hefei 230601, China
[2]China Electric Power Planning and Engineering Institute, Beijing 100120, China
[3]Department of Electrical Engineering, Fuzhou University, Fuzhou 350116, China
[4]Electrical Engineering Department, Faculty of Engineering, Minia University, Minia 61519, Egypt
[5]College of Engineering at Wadi Addawaser, Prince Sattam Bin Abdulaziz University, Wadi Addawaser 11991, Saudi Arabia
[6]College of Engineering, Sudan University of Science and Technology, Khartoum 79371, Sudan
[7]Electrical Engineering Department, Faculty of Engineering, Aswan University, Aswan 81542, Egypt

Corresponding author: Mohamed A. Mohamed (dr.mohamed.abdelaziz@mu.edu.eg)

ABSTRACT This article assesses the energy management of reconfigurable residential smart hybrid AC/DC microgrids considering the combined heat and power (CHP) loads as well as the electric vehicles charging/discharging behaviors. A holistic model is developed for the proton exchange membrane fuel cell to retrieve the unwanted thermal energy generated at the operation time. The proposed model makes use of the unoccupied capacity of the fuel cell for producing/storing hydrogen for the later usage and increasing its efficiency. A stochastic framework is designed using point estimate method (PEM) to capture the uncertainties of the photovoltaic and wind turbine forecast error, power company price, the operating temperature of the proton exchange membrane fuel cell, the price for natural gas, price for selling hydrogen, and the pressure of the H2 and O2 in the fuel cell stack. The PEM approach has shown superior advantages in terms of accuracy and running time. Considering the complex and nonlinear structure of the proposed framework, a proficient optimization technique based on the teacher learning algorithm (TLA) is devised. A two-phase modification method is proposed to increase the algorithm variety and help its convergence characteristics. The performance of the proposed algorithm is compared with the TLA, particle swarm optimization (PSO) algorithm and genetic algorithm (GA). For enhancing the security of the energy and data transaction within the system, a directed acyclic graph (DAG)-based security framework is introduced to guarantee the performance of the system against the subversive accesses. By using this scheme, the essential data of the units are recorded and secured in the form of public, private and transaction blockchains. The economic characteristics of the proposed method are assessed on a residential hybrid AC-DC microgrid test system.

INDEX TERMS Combined heat and power, smart AC-DC microgrid, point estimate method, uncertainty, energy management.

Nomenclature

BGi^t/Bsj^t	Price for i^{th} generating unit and j^{th} storage unit at t
$B^t Grid$	Price for energy company at t
$B^t PEV$	Price for energy company at t
$B_m{}^t$	Gas price for m^{th} PEMFC at t
$B^{pump,t}$	Price for Hydrogen pumping at t
B_{mHs}	Price of hydrogen selling for m^{th} PEMFC
B_m^{th}	Fuel price for the thermal demands
$Cost^{DG/ST/Grid}$	Cost of power generation by DERs/ storage unit/power company
$Cost^{PEV/SW/FC}$	Cost of power supply to PEV/cost of reconfiguration/cost of power produced by FC
C_{Bat}	Battery investment cost ($).
C_d	Degradation cost of PEV battery.

The associate editor coordinating the review of this manuscript and approving it for publication was Lin Zhang.

$C^{Sw/FC/M}$	Cost of switching/PEMFC/power company electricity
DoD_i/ DoD_f	Original/end DoD at the discharge.
E_{bat}	Battery energy (kWh)
E^{nernst}	Cell voltage in the open-circuit thermodynamic balance (no-load)
$En_{D,v}{}^t$	Electrical energy of fleet v for driving at hour t.
$En_v{}^t$	Electrical energy in PEV batteries in fleet v at hour t.
En_v^{ini}/En_v^{fin}	Primary/ending energy in fleet v.
En_v^{min}/En_v^{max}	Battery lower and upper capacity in fleet v.
H_2	Hydrogen
i^{FC}	Fuel cell current
M_{H2}	Hydrogen mass rate
$N_T/N_L/N_B$	Number of operation hours/lines/buses
N_s/N_g	Number of storage devices/generators
N_{Load}	Number of load levels
N_c/N_{dis}	Number of life/discharge cycles
N_{FC}	Number of fuel cell
$N_{P/}N_{RCS}$	Number of TLA population/ switches
N_{RCS}^{sw}	Number of daily switch operations
N_v	Number of PEV fleets
β	Number of lines needed to make a loop
O_2	Oxygen
$_{PGrid}{}^t$	Power produced by the power company at time t
$P_{Gi}{}^t/P_{sj}{}^t$	Active power output of i^{th} generator/j^{th} storage
$P_v{}^t$	Charging/discharging rate of fleet v at time t.
$P_m^{H,t}$	Hydrogen equivalent power for m^{th} PEMFC at time t
$P_m{}^t$	Power output of m^{th} PEMFC at time t
$P_m^{H,t}$	Hydrogen equivalent power at m^{th} PEMFC at time t
P_m^{Hst}	Power equivalent to stored hydrogen at m^{th} PEMFC
$P^{H-usage}$	Hydrogen equivalent power arriving PEMFC stack through the storage tank
P_m^{tht}	Thermal power generated by m^{th} PEMFC at time t
$P_m^{H,end}$	Hydrogen remained in the fuel stack at the end of the day
P^{H-max}	Stack maximum capacity minus its production
$P_{loss}{}^t$	Hourly network power losses.
$P_{c,v}{}^t/P_{d,v}{}^t$	Charging/discharging rate of fleet v.
$P_{c,v}^{min}/P_{c,v}^{max}$	Lower and upper charging rate of fleet v.
$P_{d,v}^{min}/P_{d,v}^{max}$	Min/max discharging rate of fleet v.
PD_m^{tht}	Thermal load demand of m^{th} PEMFC at time t
$P^t{}_{Load,k}$	Electric demand of k^{th} level of t^{th} hour
$P_m^{Inj,t}/Q_m^{Inj,t}$	Active/reactive power injected to bus m at time t
$P_{Gi,min}{}^t/P_{Gi,max}{}^t$	Lower and upper power capacity of i^{th} DER in hour t
$P_{FCm,min}{}^t/P_{FCm,max}{}^t$	Lower and upper power capacity of m^{th} PEMFC in hour t
$P_{sj,min}{}^t/P_{sj,max}{}^t$	Lower and upper power capacity of j^{th} storage in hour t
$P_{grid,min}{}^t/P_{grid,max}{}^t$	Lower and upper capacity of the power company at hour t
P_{charge} ($P_{discharge}$)	Charge (discharge) rate in the time interval Δt
$P_{charge,max}$ ($P_{discharge,max}$)	Upper level of charge (discharge) rate in the time interval Δt
Q	Set of all possible loops
r^{te}	Thermal-to-power energy ratio
Res^t	Spinning reserve at time t
$S_{i,\max}^{Line}$	Maximum power flow in i feeder
$S_i^{Line,t}$	Power flow in feeder i at time t
S_{Gi}^{on}/S_{Gi}^{off}	Costs of start-up/shut-down for i^{th} DER
$S_{FC,m}^{on}/S_{FC,m}^{off}$	Costs of start-up/shut-down for m^{th} PEMFC
t_m^{off}	The time at which the FC is off
τ_m	FC cooling time constant of m^{th} PEMFC
$u_i{}^t$	Status of i^{th} DERS (except PEMFC) at hour t
$u_m{}^t$	m^{th} PEMFC status at hour t
$u_v{}^t$	PEV status (charge/discharge/idle)
$u_{c,v}{}^t/u_{d,v}{}^t/u_{i,v}{}^t$	Indicator showing fleet v is in which operation mode.
V^{FC}	FC output voltage
V^{min}/V^{max}	Min/max voltage value
V/δ	Voltage magnitude/phase
V^{act}	Activation over-potential
V^{ohmic}	Voltage drop due to the resistance against the electrons for transferring on collecting plates & solid membrane
V^{con}	Voltage drop caused by the mass conveyance of the reacting gases
$W_{ess,min/max}$	Min/max battery capacity for power storage
$W_{ess}{}^t$	Battery energy at t
ω	Weighting factor for the mean value μ
X	A solution in TLA algorithm
X_T	Best individual in the TLA population
Y/Θ	Feeder admittance magnitude/ phase
S	Output vector
z	Input vector for uncertain parameters

$z_{l,1}$, $z_{l,2}$	Concentration points z_l
$\Upsilon l,3$	Skewness parameter for z_l
$\xi l,k$	Standard location for z_l
μ_{zi}	Expected value of input uncertain parameter z_l
σzl	Standard deviation for z_l
w	Line status
$Iter$	Iteration number
$\eta_{charge.discharge}$	Battery efficiency in charge or discharge mode
υ	Number of uncertain parameters
η^{st}	Hydrogen storage efficiency
$\eta_m{}^t$	FC efficiency ignoring thermal recovery and hydrogen production m^{th} PEMFC at time t
η^{tot}	Total fuel cell efficiency
μ	Mean value of random variables
κ_1 and κ_2	Wohler curve parameters in V2G
$\gamma_1,\ldots,\gamma_7$	Random amount in the range (0,1]
λ_{RCS}	Cost of switching operation
λ_m	Cost of hot start-up for m^{th} PEMFC
ϕ_m	Cost of cold start-up for m^{th} PEMFC

I. INTRODUCTION

According to the united stated DOE department, microgrid is a set of coupled loads and distributed energy resources (DERs) with specific electric borders and can act as an independent well-regulated unit from the main grid (connecting or disconnecting) to provide either grid-connected or islanded operation [1]. Therefore, it can be supposed as a small-scale self-supplied grid that can help improving the electric power quality by generation at the consumption location [2], [3]. The microgrid technology can improve the system reliability by announcing self-healing capability in the low voltage level, upgrading the power quality, diminishing air pollution, reducing power losses, increasing revenues by lower T&D investments, providing growing space for renewable energy sources (RESs), and growing energy efficacy by getting compatible with the real-time market prices [4]–[7]. In this regard, a series of researches were implemented from the earliest works in [8]–[10] to the latest works on economics, operation, planning, scheduling, control, protection, and secured data communication in microgrids [11]–[14]. On the operation and management of microgrids, some of the most well-known methods are provided in [15].

In a technical categorization, there are three types of microgrids: including AC microgrid, DC microgrid and hybrid AC-DC microgrid. Widely being studied, AC microgrids deliver AC power directly to AC and DC loads through some converters. In order to provide an optimal energy management system in the AC microgrid, an efficient control outline is developed to schedule the hybrid energy sources in [16]. The authors also pursued the optimal sizing of the proposed hybrid sources using a cuckoo search algorithm has shown to be more effective compared to genetic algorithm (GA) and particle swarm optimization (PSO). In [17], GA is used as a powerful tool for running an economic operation scheme in the AC microgrid. There are several research works published on the operation and supervision of AC microgrids and the revenues which can be attained from their interaction with the main grid [18], [19]. All-inclusive reviews on different economics aspects of AC microgrids along with their economic operation methods can be accessed in [20]. Due to the growing number of DC loads in the grids especially at the residential parts in the last years (like laptops, TVs, mobile chargers, electric vehicles, home devices, etc.), the knowledge of DC microgrid has fascinated many power engineers. In addition, lack of a synchronization system, developed efficiency and a lesser amount of power losses are some of the special features which may be provided by DC microgrids. In [21], the cost and pollution objectives are considered to construct a multi-structure in hybrid DC microgrids. In [22], an operation pattern is used seeing load and generation balance with the time of use tariff as a constraint. A holistic comparison and discussion on AC and DC structures in microgrids and the benefits of using DC one can be found in [23].

In the third group, hybrid AC-DC microgrids exist that benefit from both AC & DC technologies existing in both AC microgrids and DC microgrids. The idea of a hybrid microgrid is constructed based on the fact that it is more efficient and economical to support an AC load by an AC generating unit and a DC load by a DC generating unit. Avoiding the expensive and complex AC-DC converters is one of the main features of these grids. A mixed-integer linear model is devised in [24] which helps for scheduling of AC and DC units in a hybrid microgrid. In [25], the way of power flow control and dispatch among the units of different types in a decentralized scheme is discussed in hybrid AC-DC microgrids. In [26], an optimal energy management framework is implemented in a hybrid AC-DC topology of microgrid considering the uncertainty effects associated with wind turbine (WT) and photovoltaics (PVs) units' generation, power company and electricity demand. In [27], a min-max robust counterpart method is deployed to solve the energy management problem of hybrid microgrids. It makes use of the Taguchi's orthogonal array approach to discover the nastiest situation for modeling the uncertainties. Although these works have provided good results in the economic operation of hybrid microgrids, none of them could provide a holistic economic framework for these grids. One of the significant DC power units which is always assumed a strategic component in hybrid microgrids for stabilizing the power and demand balance in the DC side is fuel cell (FC). This DC power source can help to improve the hybrid microgrid operation not only from the electric power standpoint, but also from the thermal load standpoint. Having a high technology in the structure, thermal recovery in the proton exchange membrane fuel cell (PEMFC) can supply a valuable portion of the local thermal loads in the DC part of the hybrid microgrids. Meanwhile, optimal management strategies for scheduling the hydrogen production capability of PEMFC units can affect the operation of the microgrid sensibly. According to

recent researches, the combined heat and power (CHP) model of PEMFC can raise its efficiency by up to 70% in comparison with its electric-based model with 35-50 % efficiency [28], [29]. This fact shows the necessity of considering an efficient economic model to mend the economic operation of the hybrid microgrids. That is to say, ignoring the complete model of FCs in the hybrid microgrids can make a strategic error in the optimal operation and management of other units. Reference [30] investigated an effective economic model for a grid-connected hybrid wind-hydrogen combined heat and power systems which is able to retrieve thermal energy from the fuel cell along with proper capabilities to exchange energy with grid. Same approach is followed in [31] considering PEMFC power plant for supplying CHP loads. Also various prices are considered for energy exchange of the PEMFC to make the model more effective. In [32] the author proposed an off-grid based hybrid system comprises of renewable energy sources, FC [33] and diesel generator to handle the loads of a remote area. Also, the sizing problem of such energy sources [34] is pursued by using a discrete simulated annealing approach.

One another feature of hybrid microgrids that can greatly affect their economic operation is the possibility of changing the topology of feeders through the reconfiguration process. In the technical meaning, reconfiguration is considered as the process of grid topology reforming by means of some already installed remotely controlled switches called tie (normal open) and sectionalizing (normal closed) switches [35]. Optimal reconfiguration can benefit the microgrid from different views for example power loss saving [36], voltage level enrichment [37], load balance increase [38], reliability boost [39] and pollution reduction [40]. Unfortunately, the reconfiguration of feeders in the microgrids is not well studied by the researchers in comparison with the rich literature of microgrids with static structure. In [40], feeder reconfiguration is used to minimize the power losses in the microgrid. Neglecting RESs and the uncertainties of these DERs are some of the main shortages of this work. In [41], the positive role of reconfiguration in decreasing the AC microgrid vulnerability and increasing the operation quality are addressed. Similarly, the valuable effect of reconfiguration on minimizing the cost of AC microgrid is investigated in [42]. While these research works have studied the substantial role of the reconfiguration strategy in microgrids, none of them have considered the switching costs due to the reconfiguration. In addition, none of the above works have addressed the effect of wide spread electric vehicle charging and discharging demands on the optimal switching scheme of hybrid microgrids. This is a vital issue considering the very rapidly growing market of electric vehicles in the modern human life.

All things considered, within a smart environment, the security of the data related to the energy transactions if not properly remarked, will lead to the unauthorized malevolent accesses to the system. The necessity of providing a secure and transparent environment for energy transactions in the power system has been a matter of dispute among the researchers over the last few years. Meanwhile, the possibility of providing a secure energy transaction environment using blockchain technology has attracted much attention. In [43] the concept of blockchain is used to block cyber-attacks and providing a transparent energy transaction environment. In [44] the concept of blockchain is used in the smart cities in order to provide a secure energy transaction framework. Similar approach provided in [45]. In this regard, the authors introduced a hybrid structure which is a combination of centralized and decentralized schemes. However, there is still the possibility of data attacks exist due to the cyclic form of the blockchain and interdependency of the data blocks [46]. Authors in [46] tried to remove this drawback by proposing a directed acyclic graph (DAG) approach which will effectively reduce the chance of getting affected by the cyber attackers.

Considering the above explanations, to deal with these issues, this research work inspects the optimal operation of reconfigurable smart hybrid AC-DC microgrids considering charging and discharging of plug-in electric vehicles (PEVs) along with different types of RESs either dispatchable or non-dispatchable resources [47]–[50]. In addition, it considers a complete holistic for the PEMFC power plant to supply the thermal-electric loads. The proposed model recovers the thermal power generated by the FC stack and constructs a combined heat and power (CHP) system to meet some portion of the microgrid thermal load demand. In addition, it considers the hydrogen production ability of PEMFC to improve its overall efficiency. The target is minimizing the total cost of hybrid AC-DC microgrid operation incorporating the cost of power generation by dispatchable and non-dispatchable units, cost of power exchange between the microgrid and the power company, cost of unit start-up or shut-down, cost of switching and cost of charging/discharging of PEVs. In order to alter the consuming role of PEVs into an active role for reducing the microgrid total cost, the vehicle-2-grid (V2G) technology is used here. In addition, the cost of battery degradation is considered to avoid high discharging cycles in the PEVs. A stochastic framework is developed to include the high number of uncertain parameters including the photovoltaic (PV) and wind turbine (WT) power, the main grid power price, the operating temperature of the PEMFC, the natural gas price, the price for hydrogen selling, and the pressure of the H_2 and O_2 in the fuel cell stack. With the aim of modeling the effects of this high number of uncertainties in the problem, a stochastic framework using point estimate method is devised [51]. The proposed stochastic method replaces each uncertain parameter with a proper probability density function (PDF) and then extracts some concentration points out of these PDFs to solve the problem. As a result of the high complication, nonlinearity and mixed-integer nature of the suggested problem, a new optimization algorithm based on teacher learning algorithm (TLA) is devised to solve the problem optimally. TLA is a heuristic optimization algorithm stimulated from the teacher and students interactions in a class [52]. Furthermore, a two-phase modification scheme is

TABLE 1. A breif compariosn between references.

Reference	EVs	PEMFC	CHP Loads	Reconfigurable Hybrid AC-DC Microgrid	MTL Algorithm	Security based on DAG
[3]	✓	×	×	×	×	×
[21]	✓	×	×	×	×	×
[29]	×	✓	✓	×	×	×
[46]	×	×	×	×	×	✓
[50]	×	✓	✓	×	×	×
[52]	✓	×	×	✓	×	×
Proposed Model	✓	✓	✓	✓	✓	✓

devised which helps to raise the diversity of the algorithm and avoid premature convergence. Table 1 summarizes the above explanations.

As can be seen, this paper provides some significant novelties compared to the previous works. However, it is much more make sense to summarize the main contributions of the paper as follows:

1) Considering a complete economic model of PEMFC power plant in the optimal operation of reconfigurable hybrid microgrids.

2) Assessing the effect of PEVs on the optimal operation of hybrid AC-DC microgrids with V2G technology in a reconfigurable structure.

3) Introduction of a stochastic scheme based on TLA and point estimates to capture the uncertainties of the problem.

4) Introducing a novel two-phase modification scheme for TLA to increase its convergence rate and avoid premature convergence.

5) A secured energy and data transaction framework considered for the proposed smart AC-DC hybrid microgrid based on the DAG approach in order to improve the security and authenticity of the proposed energy management scheme. The merits and substantial performance of the proposed method are assured on a reconfigurable smart hybrid AC-DC microgrid.

II. RECONFIGURABLE SMART HYBRID AC-DC MICROGRID TECHNOLOGIES

This section explains the technology and components of hybrid AC-DC microgrids.

A. HYBRID AC-DC MICROGRID STRUCTURE

Hybrid microgrid is a promising solution to support of smart grid idea in the modern power grid architecture. Fig. 1 displays the schematic plan of a hybrid AC-DC microgrid. From Fig. 1, it is seen that a hybrid microgrid consists of two main parts of AC and DC combined in a uniform grid shape to support both AC and DC units, storages and electric consumers. The DC part of the hybrid microgrid is very suitable for connecting the DC loads like laptops, mobile chargers, electric vehicles, etc as well as DC generators such as PVs and FCs. On the other side, the AC part is compatible with AC loads such as motors and AC generators like micro turbines (MTs) and WTs.

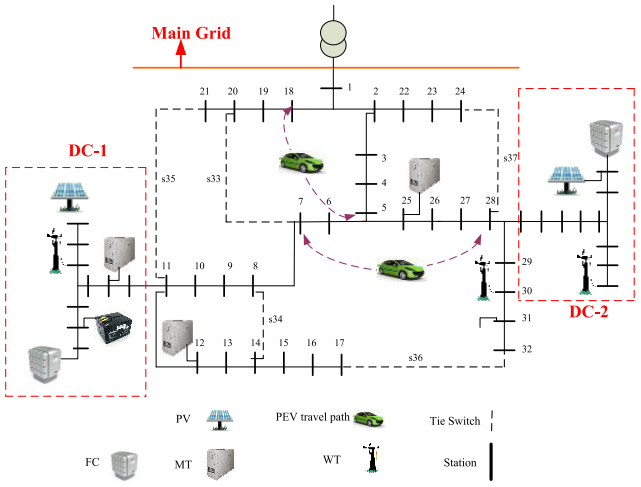

FIGURE 1. Representation of the test hybrid AC-DC microgrid.

The direct connection of AC and DC technologies into the AC and DC component of the hybrid microgrid reduces the technical power losses and the investment costs due to omitting many power electronic converters [6]. Specially, for the newly emerging technology of PEVs with the capability of both charging and discharging, the hybrid microgrid idea seems to be a very appropriate concept for the very supporting of these devices. The fast growth of RESs and PEVs clearly advocate the high success of the hybrid microgrids in the future electricity market.

B. PEV TECHNOLOGY

Each PEV fleet has some travel patterns which can be determined according to their starting point, ending point, departure and arrival times, and charging patterns [49]. The significant point is that these features can be bundled to the microgrid operation. With the purpose of changing the just-consuming role of PEVs into an active role for helping the microgrid for reducing its costs, the V2G technology can be used. In fact, the driver can let its electric car attend the V2G plan when being unused in the parking at any hour of the day. But still we should keep in mind that the PEV should have adequate energy stored for daily travels. Also, to avoid fast aging of battery, its depth of discharge (DoD) should not exceed 80%. These aging costs should be considered as an indirect cost of V2G which needs to be incorporated in the cost function. To this end, Wöhler diagram shows the maximum number of charge-discharge cycles that a battery can have before dying. Technically, the number of battery cycles before failure is calculated as follows:

$$N_{cycle}(DoD) = \kappa_1 . DoD^{\kappa_2} \tag{1}$$

where κ_1 and κ_2 are constant values adjusted according to the battery type. Table 2 reveals Wöhler diagram settings for some dissimilar batteries.

Having the Wöhler curve in hand, the battery degradation fee for $DoD = 0$ to a particular DoD_s is estimated as

TABLE 2. Wöhler parameters for four battery types [21], [22].

Type	Li-ion battery	Nickel-metal hydride (NiMH)	U.S. Advanced Battery Consortium	optimistic 2030 scenario
κ_1	1331	1515	2744	4000
κ_2	-1.825	-1.65	-1.665	-1.632

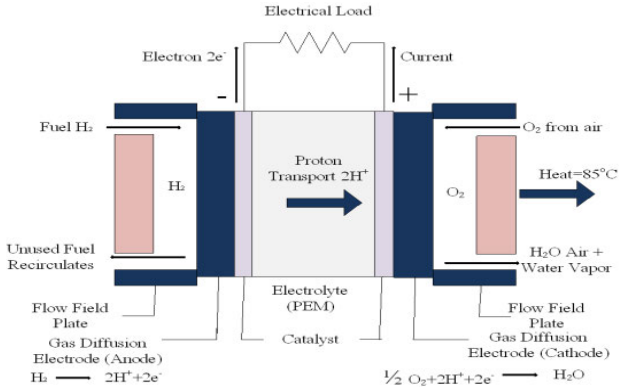

FIGURE 2. Basic PEM-FC operation.

follows [5]:

$$C_d(0, DoD_s) = \frac{C_{Bat} \times DoD_s \times E_{bat}}{N_c(DoD_s)} \tag{2}$$

Therefore, the cost of battery failure from the initial DoD_i to an end DoD_f is computed as follows:

$$C_d(DoD_i, DoD_f) = C_d(0, DoD_f) - C_d(0, DoD_i) \tag{3}$$

C. RECONFIGURABLE STRUCTURE

In a hybrid microgrid, remotely control switches come in two types, namely tie switches that are routinely open switches and sectionalizing switches that are routinely closed switches. By the use of these switches in a hybrid microgrid, one can revise the power flow pathway in the grid to reduce active losses and operation costs, improve reliability and resiliency, enhance the voltage profile and increase the power balance among different feeders. Nevertheless, due to the simple rule of avoiding high complexity in the distribution system protection, any loop needs to be opened through one of the remotely controlled switches located inside the loop. In a hybrid microgrid, the remotely control switches can play a more significant role by providing a better power dispatch opportunity when releasing feeder capacity from getting congestion issues. In addition, they can support the high penetration of RESs as well as PEVs by moving heavy loads from one feeder to another one, making space for higher power flow. In order to make use of all these benefits, reconfiguration strategy needs three main components: 1) actuators (controlling tie and sectionalizing switches), 2) communication system and 3) control center. While switches can be controlled either manually or remotely, the remotely control scheme is preferred since it provides more benefits due to fast operation.

D. FUEL CELL ECONOMIC MODEL

Proton exchange membrane FC, also named polymer electrolyte membrane FC, is a structure type of FC being designed for clean production of electricity in electric grids and transport applications. Owing to some special characteristics like low temperature (80-100°C), quick start-up, and very little noise and emission; PEMFC power plant is one of the best types of FC for the residential applications [51]. Fig. 2 displays a schematic diagram of PEMFC. The fuel of the PEMFC is hydrogen H_2 that is supplied by the reformer. A PEMFC changes the chemical energy of the fuel, the hydrogen H_2, and an oxydizer, the oxygen O_2, into the electrical power. On the cathode and anode of each cell, H_2 reacts with oxygen O_2 to create an electro-chemical reaction as follows:

$$\begin{aligned} &\text{On Anode: } H_2 \rightarrow 2H^+ + 2e^- \\ &\text{On Cathode: } \frac{1}{2}O_2 + 2H^+ + 2e^- \rightarrow H_2O \end{aligned} \tag{4}$$

Combination of the cathode and anode reactions results in the FC inside reaction as below:

$$\frac{1}{2}O_2 + H_2 \rightarrow H_2O \tag{5}$$

As it can be seen from the electro-chemical reaction, the FC output is the generation of electrons (electricity) and H_2O (vapor water). The flow of electrons on each particular cell creates the output voltage (V^{FC}) as [51]:

$$V^{FC} = E^{Nernst} - V^{act} - V^{con} - V^{ohmic} \tag{6}$$

$$\begin{aligned} E^{Nernst} &= 1.229 + 4.31 \times 10^{-5} \times T \\ &\quad \times \left[\ln(P_{H_2}) + \frac{1}{2}\ln(P_{O_2})\right] \\ &\quad - 0.85 \times 10^{-5} \times (T - 298.15) \end{aligned} \tag{7}$$

$$V^{act} = -[\xi_1 + \xi_2 T + \xi_3 T \ln(C_{O_2}) + \xi_4 T \ln(i_{FC})] \tag{8}$$

$$C_{O_2} = \frac{P_{O_2}}{5.08 \times 10^6 \times e^{(-498/T)}} \tag{9}$$

$$V^{ohmic} = i_{FC} \times (R^{elect} + R^{prot}) \tag{10}$$

$$V^{con} = -B \times \ln(1 - \frac{J}{J^{\max}}) \tag{11}$$

E. ELECTRIC POWER GENERATION

In the proposed model, a reformer is considered to extract hydrogen from the fuel with hydrocarbon. The fuel stack is fed by hydrogen, oxygen (air), and water for cooling and generates the output products including hot water and electricity. As seen in (3), each single cell generates a voltage called V^{FC}. Considering a number of series cells, the total output voltage at the stack terminal is V^T. Therefore, the electrical power generated by the cell on the load side is computed as:

$$P = V^T \times i^{FC} \tag{12}$$

F. HYDROGEN PRODUCTION STRATEGY

The amount of hydrogen generated by the reformer is partially deployed directly by the fuel stack to generate electricity and is partially stocked in the hydrogen tank for the

future demands. The core concept for considering hydrogen production in the economic model is to employ the unused FC capacity once the electric load consumption is less than the maximum capacity of the FC. To make it compatible with our electric system, P^H is defined as the equivalent electric power that hydrogen can generate at a time interval. The hydrogen mass rate of M_{H2} (in kg/s) is required to generate the amount of P^H (kW) energy using the following equation:

$$M_{H_2} = 1.05 \times 10^{-8} \left(\frac{P^H}{V^{FC}} \right) \tag{13}$$

The amount of the produced equivalent hydrogen can change in the range zero to P^{H-max} wherein P^{H-max} is the difference between the FC stack max capacity and its production. During the hours in which the thermal demand is high, the hydrogen produced is deposited in the hydrogen tank. This deposited hydrogen can be used for the generation of electricity at low thermal load hours. The unused hydrogen is sold at the end of the day. This is an economical scheme to reduce microgrid costs. The hydrogen equivalent power stored in the hydrogen tank is computed as:

$$P_t^{Hst} = P_{(t-1)}^{Hst} + P_t^H \times \eta^{st} - P_t^{H-usage} \tag{14}$$

G. THERMAL RECOVERY STRATEGY

During the operating period of the reformer, thermal energy is an unwanted output generation of the PEMFC. Since PEMFC is load-dependent, this event becomes more touchable when it is working with its high capacity. In fact, the thermal energy produced at full load becomes comparable with the amount of electric energy produced at this period. By recovering the thermal energy produced by the reformer, a CHP system is devised that can effectively support part of the thermal demands in the microgrid. The amount of generated thermal is calculated as follows:

$$P_t^{th} = r^{TE} \times \left(P_t^H + P_t \right) \tag{15}$$

Considering thermal power recovery as well as hydrogen generation, the overall efficiency of PEMFC is given by:

$$\eta_t^{tot} = \frac{P_t + \eta^{st} \times P_t^H + \min\left(P_t^{th}, PD_t^{th}\right)}{\frac{P_t + P_t^H}{\eta_t}} \tag{16}$$

where η is the FC basic efficiency (ignoring thermal and hydrogen) which is a function of the part load ratio (PLR).

III. OPERATION FORMULATION OF RECONFIGURABLE HYBRID AC-DC MICROGRID

This section gives the problem formulation consisting of the cost function and constraints.

A. PROBLEM OBJECTIVE

As previously mentioned, the microgrid encompasses different segments; the total cost of the microgrid operation would be a sum up of all its segments' costs. These costs are the cost of power supply by DERs, cost of supply to storage unit, power purchased by microgrid from the power company, startup and shutdown, switching and V2G technology which can be provided as follows:

$$Min\ E(Cost) = Cost^{DG} + Cost^{ST} + Cost^{Grid} + Cost^{PEV} + Cost^{SW} + Cost^{FC} \tag{17}$$

Cost terms are explained as follows (the operator E shows the expected value):

$$Cost^{DG} = \sum_{t=1}^{N_T} \{ \sum_{i=1}^{N_g} [u_i^t E(P_{Gi}^t) B_{Gi}^t + S_{Gi}^{on} \max\{0, u_i^t - u_i^{t-1}\} + S_{Gi}^{off} \max\{0, u_i^{t-1} - u_i^t\} \} \tag{18}$$

$$Cost^{ST} = \sum_{t=1}^{N_T} \sum_{s=1}^{N_s} E(P_{sj}^t) B_{sj}^t \tag{19}$$

$$Cost^{Grid} = \sum_{t=1}^{N_T} E(P_{Grid}^t) B_{Grid}^t + \rho \times P_{loss}^t \tag{20}$$

$$Cost^{PEV} = \sum_{t=1}^{N_T} \sum_{v=1}^{N_v} u_v^t B_{PEV,v}^t E(P_v^t) + \sum_{k=1}^{N_{dis}} C_d^k (DoD_i, DoD_f) \tag{21}$$

$$Cost^{SW} = \sum_{l=1}^{N_{RCS}} N_{RCS,l}^{sw} \lambda_{RCS} \tag{22}$$

$$\begin{aligned} Cost^{FC} = \sum_{m=1}^{N_{FC}} [& B_m^t \frac{u_m^t [E(P_m^t) + E(P_m^{H,t})]}{\eta_m^t} \\ & + S_{FC,m}^{on} \max\{0, u_m^t - u_m^{t-1}\} + \\ & S_{FC,m}^{off} \max\{0, u_m^{t-1} - u_m^t\} + B_m^{th,t} \\ & \times \max\left\{ E(PD_m^{th,t}) - E(P_m^{th,t}), 0 \right\} + \\ & u_m^t B_m^{pump,t} \eta_m^{st} E(P_m^{H,t}) \\ & + \alpha_m + \phi_m \left(1 - \exp\left(\frac{t_m^{off}}{\tau_m} \right) \right) - B_m^{Hs} E(P_m^{H,end})] \end{aligned} \tag{23}$$

In the above formulation, (18) covers the cost of power generated by DERs (except FC which is discussed in more detail in (23)) and startup and shutdown cost. The startup and shutdown cost are covered by the term $\max\{0, u_i^t - u_i^{t-1}\}$ which makes the startup cost S_{Gi}^{on} to be imposed to the problem if and only if the generator is off at *t-1* and on at t. Same definition is valid for the shutdown cost S_{Gi}^{off} if the generator is on at *t-1* and off at t. Equation (19) calculates the battery storage energy cost, (20) calculates the cost of power bought from the power company. Equation (21) is made up of two different terms. The first term defines the cost of PEVs' exchange power. The second one expresses the aging cost of the batteries due to their consistent charging/discharging cycles. Equation (22) evaluates the aging cost of switches during the

reconfiguration wherein the number of switching operations, i.e., either opening or closing, is calculated. Equation (23) calculates the cost of power generated by PEMFC which comprises of seven different terms. The first term shows the cost of electric power produced by PEMFC. The second and third terms are the cost of startup and shutdown, respectively. Cost of fuel supply for the thermal loads is represented by the term number four. The fifth term indicates the cost of pumping hydrogen into the system and the cost of cold and hot start-up are shown by the terms number six and seven. The last term in (23) shows the benefit of selling additional hydrogen to the grid at the end of the day.

B. PROBLEM CONSTRAINTS

The above cost function is optimized considering the technical operation constraints as explained in the rest.

-Electricity Load and Power Balance: A hybrid microgrid has an AC area and a DC area. In the DC area, the power and demand load balance is preserved as follows:

$$\sum_{i=1}^{N_g} E(P_{Gi}^t) + \sum_{j=1}^{Ns} E(P_{sj}^t) + \sum_{m=1}^{N_{FC}} E(P_m^t) + E(P_{Grid}^t) = \sum_{k=1}^{N_{Load}} E(P_{Load,k}^t) \quad (24)$$

In the AC sector of the microgrid, the generation and demand balance constraint is preserved as:

$$E(P_m^{Inj,t}) = \sum_{n=1}^{N_B} E(V_m^t)E(V_n^t)Y_{mn}\cos\left(\Theta_{mn} + E(\delta_m^t) - E(\delta_n^t)\right) \quad (25)$$

$$E(Q_m^{Inj,t}) = \sum_{n=1}^{N_B} E(V_m^t)E(V_n^t)Y_{mn}\sin\left(\Theta_{mn} + E(\delta_m^t) - E(\delta_n^t)\right) \quad (26)$$

- DESs Capacity Limit:

$$\begin{aligned} P_{Gi,\min}^t &\le E(P_{Gi}^t) \le P_{Gi,\max}^t \\ P_{sj,\min}^t &\le E(P_{sj}^t) \le P_{sj,\max}^t \\ P_{FCm,\min}^t &\le E(P_m^t) \le P_{FCm,\max}^t \\ P_{grid,\min}^t &\le E(P_{Grid}^t) \le P_{grid,\max}^t \end{aligned} \quad (27)$$

- PEMFC Hydrogen Generation Capacity:

$$0 \le P_{mt}^H \le P_{mt}^{H-\max} \quad (28)$$

- Storage Unit Limits:

$$E(W_{ess}^t) = E(W_{ess}^{t-1}) + \eta_{charge}E(P_{charge})\Delta t - \frac{1}{\eta_{discharge}}E(P_{disch\,arg\,e})\Delta t$$
$$\begin{cases} W_{ess,\min} \le E(W_{ess}^t) \le W_{ess,\max} \\ E(P_{charge,t}) \le P_{charge,\max} \\ E(P_{discharge,t}) \le P_{discharge,\max} \end{cases} \quad (29)$$

- Spinning Reserve:

$$\sum_{i=1}^{N_g} u_i^t E(p_{Gi,\max}^t) + \sum_{j=1}^{Ns} u_j^t E(p_{sj,\max}^t) + \sum_{m=1}^{N_{FC}} u_m^t E(p_{m,\max}^t) + \ldots$$
$$E(P_{loss}^t)E(p_{grid,\max}^t) \ge \sum_{k=1}^{N_{Load}} E(P_{Load,k}^t) + E(P_{loss}^t) + Res^t \quad (30)$$

- Feeder Capacity:

$$|E(S_i^{Line,t})| < S_{i,\max}^{Line} \quad (31)$$

- Bus Voltage Limit:

$$V_m^{\min} \le E(V_m^t) \le V_m^{\max} \quad (32)$$

- Keeping the Microgrid Radiality: To avoid loop formation and at the same time avoiding making any bus islanded, (33) is considered. Therefore, for any loop including β lines, only $\beta - 1$ lines can remain charged:

$$\sum_{q\in Q} w_{it} = \beta_q - 1 \quad (33)$$

The symbol w can take 0 or 1 representing the line status of open or closed, respectively.

- PEV Charge/Discharge/Idle Mode of Operation:

$$u_{c,v}^t + u_{d,v}^t + u_{i,v}^t = u_v^t \quad (34)$$

- PEV Fleet Maximum/Minimum Charging Rate:

$$u_{c,v}^t P_{c,v}^{\min} \le E(P_{c,v}^t) \le u_{c,v}^t P_{c,v}^{\max} \quad (35)$$
$$u_{d,v}^t P_{d,v}^{\min} \le E(P_{d,v}^t) \le u_{d,v}^t P_{d,v}^{\max} \quad (36)$$

- PEV Energy limits:

$$E(En_v^t) = E(En_v^{ini}) + \sum_{m=1}^{t}(u_{c,v}^m E(P_{c,v}^m)\eta_{c,v} - u_{d,v}^m E(P_{d,v}^m)\eta_{d,v}) - \sum_{m=1}^{t}(1 - u_v^m)E(En_{D,v}^m) \quad (37)$$

- PEV Fleets' Energy Capacity: Each PEV fleet can provide a maximum amount of energy to discharge into the hybrid microgrid at each hour as (38)-(39). Also, it is assumed that the amount of PEV energy at the first hour and the last hour of the day should stay the same as (40):

$$E(P_v^t) = E(En_v^t) - E(En_v^{t-1}) \quad (38)$$
$$En_v^{\min} \le E(En_v^t) \le En_v^{\max} \quad (39)$$
$$E(En_v^{fin}) = E(En_v^{ini}) \quad (40)$$

- Initial PEV Fleet Energy:

$$En_v^{t'} = En_v^{\max} \quad (41)$$

To make it crystal clear, Fig. 3 depicts the inputs, outputs and the methodology.

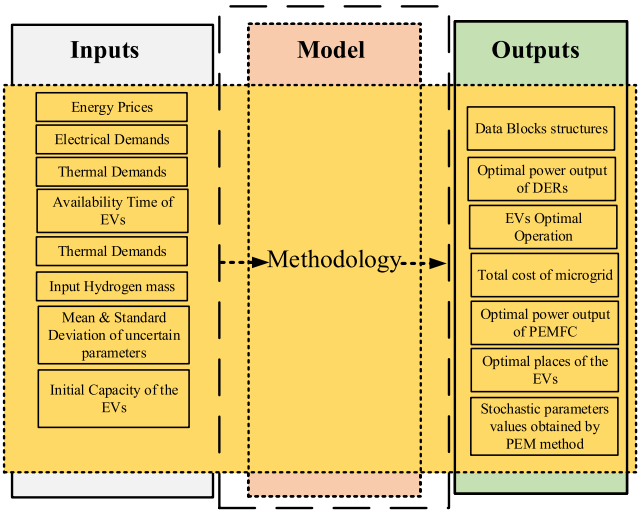

FIGURE 3. The methodology, inputs and outputs of the model.

Also, the microgrid is a radial system; hence, the operation cost due to the active loss of the AC system is unavoidable and can be represented as follows:

$$Cost^{Loss\_MG} = \sum_{L=1}^{N_L} \left(R_L \times I_L^2\right) \times C^{Loss\_MG} \tag{42}$$

IV. STOCHASTIC FRAMEWORK BASED ON MTLA AND POINT ESTIMATES

This section explains two elements of the proposed stochastic framework, namely MTLA and PEM which are explained in the rest.

A. POINT ESTIMATE METHOD

The point estimate method has found much popularity due to its powerful ability and accuracy in modeling the uncertainty. The original point estimate method needs 2^{υ} algorithms to find the statistical moments of an uncertain data [52], [53]. Here υ is the quantity of problem uncertain parameters. In [54], Hong simplified the point estimate method by lessening the number of runs from 2^{υ} to K and $K\upsilon+1$, wherein $K\upsilon$ is Hong's scheme. Lastly, in [55], Su showed that Hong's 2υ scheme is the most appropriate method for usage in the power flow problem. The main feature of 2υ point estimate method is that it is constructed on the statistical data of the uncertain parameter counting the average, variance and skewness to model the uncertainty. In this regard, it first replaces the uncertain parameter with a fitting PDF. Then the stochastic problem is changed to 2υ deterministic sub-problems with different probability levels. So as to develop the mathematical formulation, the problem equations are supposed as a nonlinear function:

$$S = F(z) \tag{43}$$

Based on (43), the feeding uncertainty z is reflected to the output results S over the nonlinear equation F. To include the uncertainty in the problem, the uncertain parameter z_l is replaced with a proper PDF f_{zl}. Considering the mean, standard deviation and skewness value of the PDF, 2υ point estimate method extracts two concentration points z_{l1} and z_{l2} as follows:

$$z_{lk} = \mu_l + \xi_{lk}.\sigma_l \quad k = 1, 2 \tag{44}$$

$$\xi_{lk} = \frac{\Upsilon_{l3}}{2} + (-1)^{3-k}\sqrt{\upsilon - \left(\frac{\Upsilon_{l3}^2}{2}\right)^2} \quad k = 1,\ 2 \tag{45}$$

The skewness parameter Υ_{l3} is evaluated as below:

$$\Upsilon_{l3} = \frac{E\left[(z_l - \mu_l)^3\right]}{(\sigma_l)^3} \tag{46}$$

Each concentration point constructs a deterministic framework in which the stochastic problem is solved. Finally, the standard deviation and the expected value of the output S_i is computed:

$$\sigma = \sqrt{var(S_j)} = \sqrt{E(S_j^2) - \left[E(S_j)\right]^2} \tag{47}$$

$$E(S_j^s) = \sum_{l=1}^{\upsilon}\sum_{k=1}^{2}\left(\frac{1}{2\upsilon} \times S_j^s(\mu_1, \mu_2, \ldots, z_{lk}, \ldots, \mu_\upsilon)\right) \tag{48}$$

B. MODIFIED TEACHER LEARNING ALGORITHM

Owing to the hard, constraint and nonlinear nature of the formulation explained in section III, a novel optimization algorithm based on MTLA is presented in this part. TLA is a metaheuristic optimization algorithm mimicking the teacher and student relationships in a class. The main feature of TLA is having few adjusting parameters and high search ability for solving mixed-integer nonlinear optimization problems. In TLA, the population is divided into two groups of teachers and students. Similar to the other meta-heuristic algorithms, an initial population is created. Once computing the cost objective of all members, the best one is set as teacher X_T. From now on, the algorithm makes use of two stages to upgrade the population for several iterations. These two stages are termed teacher stage and student stage. At the teacher stage, the teacher tries to help students progress their knowledge. In the learner stage, students try to improve their knowledge amongst themselves by interaction, discussion, etc. Each of these two stages is simulated mathematically as follows:

Teacher stage: In order to simulate this phase, first the average of the class is calculated M_S. Then, the mean of the population is moved toward X_T as follows [43]:

$$M_S = [m_1, m_2, m_3, \ldots, m_N] \tag{49}$$

$$X^{Iter+1} = X^{Iter} + \gamma_1(X_T - T_F M_S) \tag{50}$$

If the current position is superior to the old one, then replace it. Here T_F is an accelerating parameter getting 1 or 2, randomly.

Student stage: For simulating the learner phase, the interaction among friends in a class should be simulated.

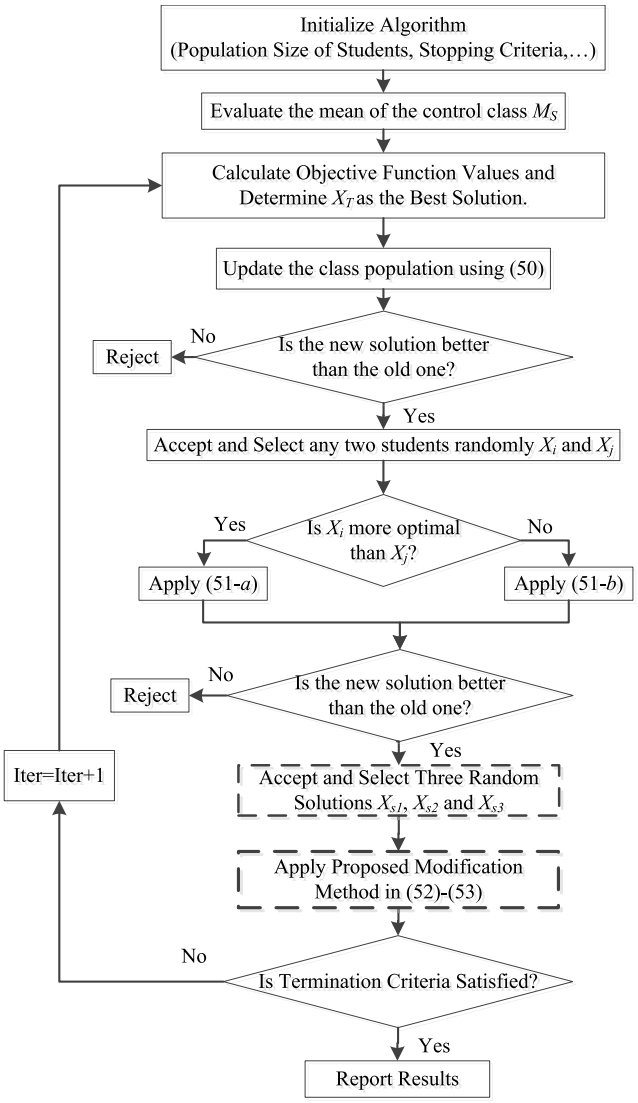

FIGURE 4. Flowchart of the proposed MTLA.

Therefore, for any two random individuals X_i and X_j, the following math operation is implemented:

for $i = 1{:}N_P$

If $F(X_i^{Iter}) \prec F(X_j^{Iter})$

$$X_i^{Iter+1} = X_i^{Iter} + \gamma_2(X_i^{Iter} - X_j^{Iter}) \quad \text{(51-a)}$$

If $F(X_i^{Iter}) \prec F(X_j^{Iter})$

$$X_i^{Iter+1} = X_i^{Iter} + \gamma_3(X_j^{Iter} - X_i^{Iter}) \quad \text{(51-b)}$$

End *if*

End *for*

The flowchart of the algorithm is shown in Fig.4. This paper proposes a new modification method for TLA to empower the search ability of the algorithm and reduce the possibility of premature convergence. The proposed two-phase modification method is explained in the rest:

Modification method one: This modification technique is built based on the crossover operator and mutation operator from GA. It can increase the students' diversity and thus reduce the possibility of premature convergence. For each student X_i, three random solutions X_{s1}, X_{s2} and X_{s3} are picked randomly in the way $s_1 \neq s_2 \neq s_3 \neq i$. Therefore, a mutated solution can be produced as follows:

$$X^{mut} = X_{s1} + \gamma_4 \times (X_{s2} - X_{s3}) \quad (52)$$

Using the crossover operator, three test solutions can be generated as below:

$$x_j^{test1} = \begin{cases} x_{mut,j} & if\ \gamma_5 \leq \gamma_6 \\ x_{T,j} & if\ \gamma_5 \leq \gamma_6 \end{cases}$$

$$x_j^{test2} = \begin{cases} x_{mut,j} & if\ \gamma_6 \leq \gamma_7 \\ x_{s,j} & if\ \gamma_6 \leq \gamma_7 \end{cases}$$

$$X^{test3} = \phi \times X_T + \lambda_8 \times (X_T - X_{mut}) \quad (53)$$

The most optimal solution among X^{test1}, X^{test2}, X^{test3} and X_s is located in the population. This process continues until the time that all the class is updated.

Considering the fact that the optimization algorithms are highly dependent to the systems' sizes and numbers of variables, most of the methods are not able to find the global solution when faced with high number of variables in the problem. In contrary to such methods, the proposed MTLA algorithm is highly effective in case of complex problem with high number of variables.

C. SOLUTION PROCEDURE

In order to apply the point estimate method and MTLA on the proposed formulation, these steps are required:

Step 1: Enter the hybrid microgrid information including the branch data, bus data, voltage level, DGs characteristics, etc, the optimization algorithm data (student population size and termination criterion) and stochastic model (the mean and standard deviation of the uncertain parameters).

Step 2: Initialize the student population. Each student X represents a feasible solution for the problem in hand.

Step 3: Calculate the expected value of the cost function (17) based on point estimate method. To this end, equations (44)-(48) are implemented to find the expected value of cost function.

Step 4: Choose the solution with the least expected cost function value as teacher X_T and store it.

Step 5: Apply the teacher phase as in (49)-(50) to improve the student population.

Step 6: Apply the learners' phase as in (51) to improve the student population.

Step 7: Apply the modification phase as in (51)-(53) to improve the student population.

Step 8: Update the teacher according to the new improved population.

Step 9: Check the termination criterion, if satisfied finish the algorithm and go to the next step otherwise return to step 5.

Step 10: Finish the algorithm and publish the results.

V. DAG BASED SECURITY FRAMEWORK

The concept of centralization of authority suffers from the absence of transparency of the data-sharing mechanism among the third party nodes. Blockchain basically created to provide a secured, transparent and trusted data transaction between untrusted entities in a system. Blockchain is a distributed ledger which is powered by the nodes of the system which hold the transactions of the ledger processed by the nodes of the system. The underlying of the distributed ledger is the blockchain technology through which the transactions are gathered into data blocks and broadcasted across the system comprises of the proposed nodes. The chain of the data blocks forms the blockchain concept. The each new transaction in the system will be added to the list of records held by the blockchain in the form of data blocks. The consecutive data blocks are linked together and secured using the cryptography. The data blocks have different sections as can be seen in Fig. 5. In this regard, each new data block is sealed with a *hash code* which is the hash version of the previous block's header [43]. On the other hand, the header of the previous block will be turned into a hash address and attached to the new data block. Such correlated mechanism enhances the security of the shared data within the system and frustrates any malicious unauthorized access, target of which is either to inject any useless data or change the data blocks since it will be immediately inferred by the nodes.

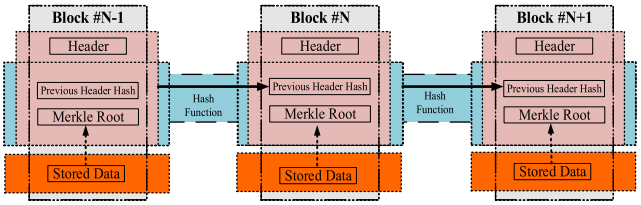

FIGURE 5. Illustrative representation of Blockchain structure.

Recently, the concept of blockchain is adopted by the researchers for enhancing the security of the energy and data transactions within the power systems. In this regard, the power system's agents either the producers or demands are considered as the nodes of the system where they should broadcast the data related to their transactions through the data blocks to the blockchain which the agents are capable to access and make the transactions transparent. Although the blockchain improves the safety of data transactions, still some challenges exist with such technology. One issue is that the accuracy of calculating the hash addresses (HAs) will be decreased in a system filled with nodes and agents. Another issue is that there still the possibility of unauthorized access exists due to the cyclic form of the blockchain through a third party entity. To remove these weaknesses, the concept of directed acyclic graph (DAG) approach is provided by the researchers in energy-oriented environments [46]. The DAG approach enables the data blocks to be transacted in a proper categorized based manner. In this regard, the DAG approach enables the public, private and transaction data of the agents of the system to be broadcasted through the *public blockchain*, *private blockchain* and *transaction blockchain*, respectively. The public blockchain holds the public information of the agents which is transparent and open for any other third-party entity. On the contrary, the private blockchain is only accessible for a few nodes of the system which demands the credibility of the nodes if any of the nodes decide to add a new data block. The transaction blockchain handles the data related to the transactions between the agents. On the other hand, any transaction between the nodes of the system will be broadcasted to the transaction blockchain.

Please note that this paper is proposing a new architecture for hybrid AC-DC microgrids to consider the cyber-physical requirements of energy management in these systems. Keep it in the mind that most of the available works in the area of energy management of hybrid microgrids have only considered the physical layer, the security of data transaction in practical cases is so vital. This necessitates considering the cyber layer, appeared as a DAG based approach, in the analysis. The numerical results are not affected if the cyber layer is ignored as long as it is assumed that all data transactions are secure and have not been compromised or changed. Without a reliable and secure data transaction scheme, it is always possible that the entire energy management be affected by malicious players. Therefore, apart from the energy management scheme of the paper (so-called physical layer), a secured data transaction framework (cyber layer) is also provided in this paper and these two concepts are interrelated. This provides a secure platform for the data related to the energy transactions in the hybrid AC-DC system.

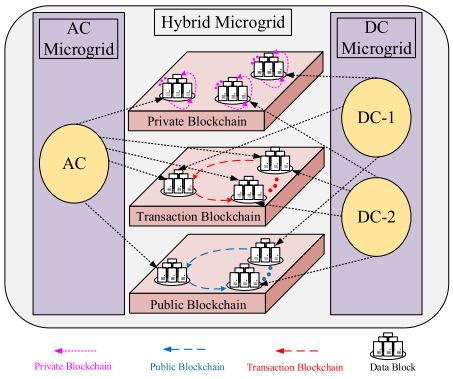

FIGURE 6. DAG based data transaction within smart hybrid AC-DC.

In this paper, the concept of DAG approach is provided for the proposed hybrid AC-DC microgrid. Fig. 6 depicts the detail of the DAG framework among the agents of the system. As can be seen, the public, private and transaction data of the nodes will be transmitted independently. The unique cyclic of the blockchain does no longer remain which will diminish the possibility of data attacks. In this case, the collected new data which is intended to be transmitted through a new data blocSk by the nodes will be formed and secured using merkle root mechanism and embedded in the block header [43]. The block header of current data block will be transformed into

a HA using SHA-256 hash function [43] and served as the "*previous hash*" of the next data block.

VI. SIMULATION RESULTS

In this section, the proposed approach is tested on a microgrid considering different types of DERs such as WT, PV, FC and MT. The test system is the IEEE 33-bus grid including 5 tie switches and 31 sectionalizing switches. The hybrid microgrid has one AC part and two DC parts which are connected to each other on buses 11 and 28 as shown in Fig. 1. The tie switches are shown by back dotted line in this figure located at lines 7-20, 8-14, 11-21, 17-32, and 24-28. The other switches are kept closed, making the grid ready for reconfiguration. The DC and AC components of the microgrid are joint to each other by means of proper converters. The AC and DC parts of the microgrid have a voltage level of 12.66 (kV) and 1 (kV), respectively. The whole data of the grid are provided in [56]. The AC and DC parts of the hybrid microgrid will exchange power with each other depending on the economic benefits. The location of DERs is shown in Fig. 5 and their complete data are provided in Table 3. Regarding the PEVs, two fleets are considered in the grid with travel paths as shown in Fig. 5. Other data regarding the time and locations of PEV fleets are provided in Table 4. The PEV fleet's capacity and charging/discharging rates are revealed in Table 5. For reconfiguration, each switching operation is assumed to cost 1($). There is one PEMFC located in the hybrid microgrid for which the complete data are shown in Table 6.

TABLE 3. Characteristics of the DERs in the Hybrid Microgrid.

Type	Min Capacity (kW)	Max Capacity (kW)	Bid (€ct /kWh)	Start-up/Shut-down cost (€ct)
PV-1	-	100	2.584	0
MT-1	25	260	0.457	0.448
Battery	-180	180	-	-
PEMFC	30	260	0.294	1.65
WT-1	-	155	1.073	-
DC MG1-ACMG	-200	200	-	-
MT-2	50	250	0.457	1.65
MT-3	65	250	0.457	1.65
WT-2	-	250	1.073	-
PV-2	-	200	2.584	0
FC-2	0	400	0.294	1.158
WT 3	-	300	1.073	0
DC MG2-AC MG	-250	250	-	-

For the sake of simplicity, similar wind power patterns are assumed for WT but with different capacities. The forecast values of WT, PV, load demand power factor in DC1, DC2 and AC parts of the hybrid microgrid and the market price are shown in Fig. 7. The analysis is done for 24 hours. In order to have a better comparison, three different operation cases (OCs) are provided:

OC-1: Optimal operation of the hybrid microgrid ignoring reconfiguration and detailed PEMFC model.

OC-2: Optimal operation of the hybrid microgrid considering reconfiguration but still ignoring the detailed PEMFC model.

TABLE 4. Travel characteristics of PEVs.

Fleet Number	First Travel				Second Travel			
	Departure		Arrival		Departure		Arrival	
	Time	Bus	Time	Bus	Time	Bus	Time	Bus
1	5:00	5	6:00	18	17:00	18	18:00	5
2	6:00	7	7:00	28	17:00	28	18:00	7

TABLE 5. PEV fleet characteristics.

Fleet	Capacity (kWh)		Charge/Discharge rate (kW)	
	Min	Max	Min	Max
1	234.0	2973.0	7.3	496.0
2	344.0	2644.0	7.3	292.0

TABLE 6. The characteristics data of PEMFC unit.

Parameter	Value
T	333k
P_{H2}	1 (atm)
P_{O2}	0.2095 (atm)
B	0.016
ξ_1	-0.948
ξ_2	0.00286+0.0002 ln(0.0064)+ ln(C_{H2})
ξ_3	7.6×10^{-5}
ξ_4	-1.93×10^{-4}
J_{max}	469 mA/cm^2
Fuel price for residential loads	0.29 (€ct /kWh)
Hydrogen Selling Price	9.44 (€ct /kWh)
Hydrogen storage efficiency (η_{st})	0.95(€ct /kg)
Hydrogen pumping cost	0.09 (€ct /kWh)
FC cooling time constant	0.75
Hot startup cost	0.26 (€ct)
Cold startup cost	0.7 (€ct)

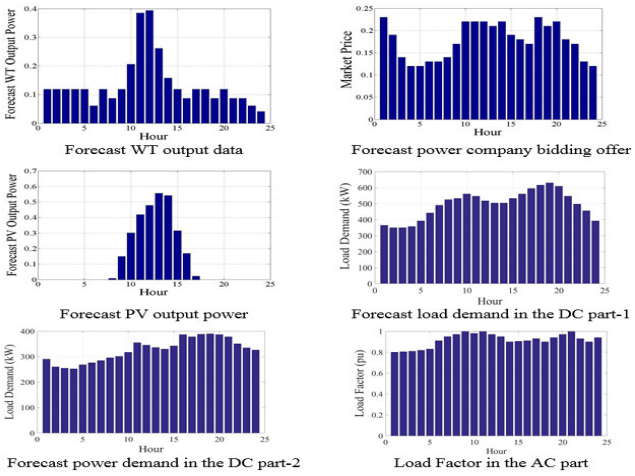

FIGURE 7. WT, PV, price and load demand forecast data.

OC-3: Optimal operation of the hybrid microgrid considering both reconfiguration and detailed PEMFC model.

Table 7 presents the simulation results for all scenarios. In order to investigate the search ability of the proposed MTLA and have a better assessment, the results of GA,

TABLE 7. Cost objective function comparison at three different OCs with for four different algorithms.

Case	GA	PSO	TLA	MTLA
OC-1	77119	76841	76740	76482
OC-2	76203	75896	75841	75504
OC-3	75104	74608	74525	74203

particle swarm optimization (PSO) algorithm and conventional TLA are used as benchmarks. To make it more clarify, although the GA algorithm is an accurate method, it has a long running time, due to the high time consuming process of generating new populations. Also, the accuracy of such method is highly sensitive to the controlling parameters of the GA. Please note it that the main feature of MTLA over the other well-known algorithms such as PSO and GA is that it does not have any specific setting parameter like weighting factor and learning factor. The inertia weight w and learning factors C1 and C2 exist in PSO algorithm, which are the main control parameters of this algorithm. Through these parameters, the behavior and efficacy of the PSO method are determined. As it can be seen from below, the weighting factor w determines the weight of the particle speed in updating its new position. The learning factors, also called accelerating factors, determine that how much confidence the particle has on its own self (parameter C1) and how much confidence a particle has on its neighbors (parameter C2). In this paper and after several running of the algorithm, for PSO algorithm, the initial number of particles and generations equals 40 and 1000 respectively. Also, the maximum velocity and the inertia weight factor are set 2 and 0.8 respectively. For GA, the crossover and mutation probability are chosen 0.8 and 0.08, respectively. Also, the initial population equals 60 individuals with 200 iterations. It should be noted that all algorithms were left to make sure do not show any more progress in their performance. Therefore, the maximum number of iterations is according to their most optimal progress. For MTLA algorithm, there is no specific setting parameter. The only parameter is the maximum iteration number which is supposed to 100 and the class size is 25.

By comparing OC3 with OC2 and OC1, the positive roles of reconfiguration and PEMFC detailed model in reducing the total costs are clear. In fact, reconfiguration strategy could alter the power flow path in the hybrid microgrid not only to reduce power losses but also to provide better opportunity for DERs to produce power at a more optimal point. For PEMFC, the lower cost value is due to the thermal power recovery and hydrogen storage which can both benefit the microgrid, economically. Also, it is seen that MTLA shows superior performance than the other well-known algorithms by getting into more optimal solutions in all cases. This proves the high search ability of the proposed MTLA.

With the intention of better understanding of the optimal scheduling point of the hybrid microgrid, Fig. 8, 9 and 10 illustrate the optimal power generation of units in areas DC1, DC2 and AC of the hybrid microgrid. It should be noted that due to the successful role of reconfiguration and PEMFC on the microgrid performance, only the results of OC-3 are discussed in the rest. According to these figures and in the area DC-1, the PEMFC is producing more than the other units. The reason is that this unit can generate thermal power which is recovered in our detailed model and is used for supplying part of the thermal load. This is discussed in more detail in Fig. 10. Also it is seen in Fig. 8 that the battery is charging the first hours of the day at low-price hours and then discharge later at peak hours when the power company price is expensive. For RESs such as PV and WT, they produce with their maximum power capacity due to the incentive policy of supporting renewable energy. In both Figs. 8 and 9, the DC areas of the hybrid microgrid could supply their power demand using their internal DERs at low-load times, like at the start of the day. But, in the middle of

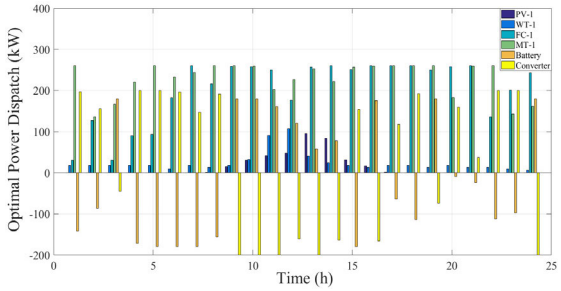

FIGURE 8. Power dispatch of DERs in area DC-1 of the hybrid microgrid in OC-3.

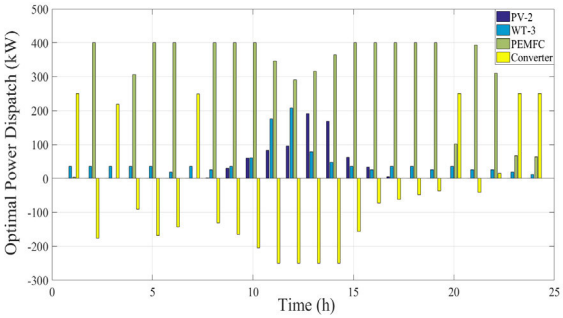

FIGURE 9. Power dispatch of DERs in area DC-2 of the hybrid microgrid in OC-3.

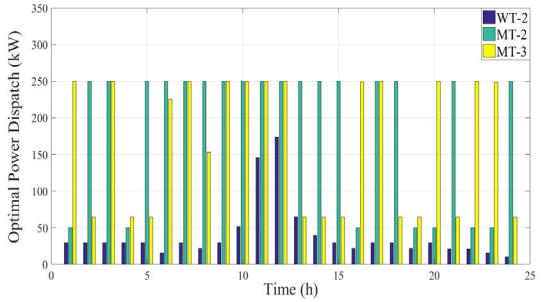

FIGURE 10. Power dispatch of DERs in AC part of the hybrid microgrid in OC-3.

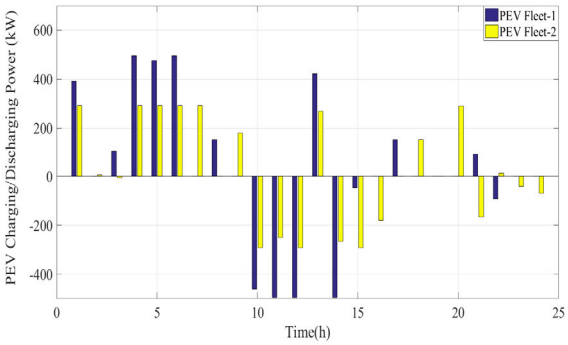

FIGURE 11. PEV charging and discharging status in the hybrid microgrid in OC-3.

the day when the power demand increases, some amount of power is purchased from the AC area which is shown by the negative sign in converters. At the AC area of the microgrid in Fig. 10, it is seen that MTs with the same characteristics are producing different amount of power. This is due to their different locations at the microgrid which limits the possibility of power injection at some hours. Also, since the AC part of the microgrid does power exchange with both DC areas as well as the main grid, it is quite a nonlinear relationship which is determined according to the economical preference as in (17)-(23).

The PEV fleet power charging and discharging status are shown in Fig. 11. It is worth mentioning that the positive values show the charging power and the negative values are discharging power of the PEVs. According to this figure, both fleets are charging at the beginning of the day to store adequate energy for discharging in the middle of the day when it is too expensive for purchasing power from the main grid. Obviously, since the EVs in fleet-1 are of higher capacities than the fleet-2, the EVs are much more occupied in the operation to make the most out of their free capacities. This helps the microgrid to cut its operation costs, greatly. Such a wise economic policy is granted due to the V2G technology which makes it possible to change the role of PEVs from only consumers to active players in the grid for producing power. It is seen that at hours which PEVs are on the road, there is no charging/discharging happening.

In order to better focus on the PEMFC model, the results of this unit are specifically discussed in the rest. In Table 8, the PEMFC efficiency before and after considering hydrogen generation and thermal recovery are shown. The basic efficiency shows the traditional model of PEMFC when this unit is only used as an electric power generator. On the opposite, the ''overall efficiency'' term shows the PEMFC efficiency incorporating the thermal power and hydrogen generation polices. According to these results, the FC efficiency is improved in all hours, effectively. Such a great improvement shows the necessity of considering complete economic model in the analyses.

In order to better see the behavior of PEMFC in supporting thermal loads, Fig. 12 shows the comparative plot of

TABLE 8. PEMFC Efficiency Including Hydrogen Generation and Thermal Recovery in OC-3.

Time (h)	1	2	3	4	5	6	7	8
Basic Efficiency (%)	40.8	37.3	40.8	38.9	38.8	33.8	28.3	30.3
Overall Efficiency (%)	67.6	64.3	66.5	65.1	64.9	60.6	56.8	56.6
Time (h)	9	10	11	12	13	14	15	16
Basic Efficiency (%)	28.2	28.2	28.0	34.3	28.2	28.3	28.0	28.3
Overall Efficiency (%)	56.4	56.3	55.2	61.5	56.1	56.8	55.2	56.8
Time (h)	17	18	19	20	21	22	23	24
Basic Efficiency (%)	28.3	28.3	28.0	28.2	28.3	36.9	32.0	28.2
Overall Efficiency (%)	56.8	56.8	55.1	56.4	56.8	63.9	58.4	54.8

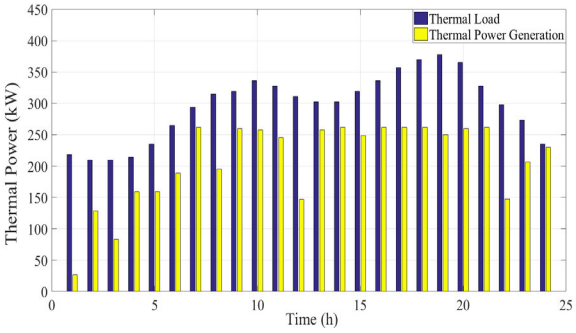

FIGURE 12. Comparative plot of thermal load demand and thermal power generation by the PEMFC.

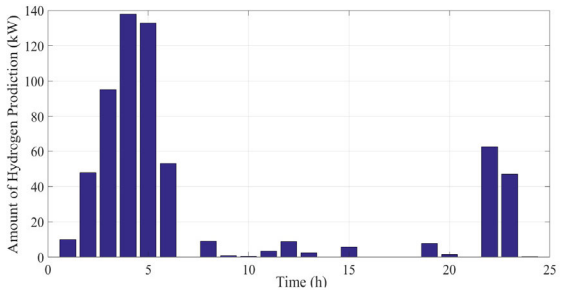

FIGURE 13. Hydrogen produced by the PEMFC in OC-3.

thermal load demand and thermal power generation at different hours. According to the bar diagrams, the unwanted thermal power generated by the FC is now supplying a big portion of the thermal load at the DC area. This is so economical for the microgrid and reduces its operating costs. Finally, Fig. 13 shows the amount of hydrogen generated by the PEMFC during the operation time horizon. As mentioned before, the FC unit can produce and store hydrogen when it has some unused capacity for power generation. Therefore, it is seen that the FC is generating hydrogen at the beginning hours of the day when there is an unused power generation capacity available. But, in the middle of the day when the microgrid is heavy loaded, FC uses its maximum capacity to generate electrical power and helping the microgrid for less power purchasing from the main grid.

Finally, the reconfiguration results are shown in Table 9. This table shows the status of open switches, meaning that all

TABLE 9. Optimal reconfiguration results in the Hybrid AC-DC Microgrid.

	Time (h)	1	2	3	4	5	6	7	8
Tie switches	1	33	33	20	33	20	33	20	33
	2	14	34	34	14	14	12	14	12
	3	21	35	35	35	35	35	21	35
	4	15	15	36	32	36	36	36	15
	5	37	37	37	24	22	37	24	24
	Time (h)	9	10	11	12	13	14	15	16
Tie switches	1	6	33	33	20	33	20	7	20
	2	14	34	34	34	12	14	34	34
	3	21	8	35	35	35	35	10	35
	4	15	36	15	15	32	32	36	32
	5	37	37	37	24	37	37	37	37
	Time (h)	17	18	19	20	21	22	23	24
Tie switches	1	7	33	33	20	20	20	33	20
	2	14	34	14	14	12	34	13	34
	3	8	35	35	35	35	35	8	8
	4	36	15	36	36	17	32	36	32
	5	37	22	37	24	37	37	37	37

TABLE 10. Data block framework for dc-1 microgrid at t = 13.

Block1				
Private			Public	Transaction
Previous HA			Previous HA	Previous HA
A21de8bb112351bccd63ee913256371a			A2da1ee214217bba32dee125292664b1	3e6a81bb235abebacf55aa862114232b1
Current HA			Current HA	Current HA
3a4dd1bc461164bfda3eeb152546163b			Ea23a5aa4223aabbfe5abb542369962b2	Fea1c3aa217667afda6daa264112531f2
PV-1 (KW)	PEMFC (KW)	MT (KW)	Total generation (KW)	Converter
98	263	260	621	-200

TABLE 11. Data block framework for dc-2 microgrid at t = 20.

Block1			
Private		Public	Transaction
Previous HA		Previous HA	Previous HA
3ead12bc874963bfda0aac14785616a5		Fas4785fc1582aacffeac5badf369fcfbf	Acf1c3fc236c12afda6daadef118961aa
Current HA		Current HA	Current HA
Ab53b6ee392312bbce677a562345921a		Deeea5aa231159bffa6dea462132172b2	Ae4bb11abb1463bdda6deb963245461a
FC-2 (KW)	WT-3 (KW)	Total generation (KW)	Converter
101	46	147	250

other switches are closed at the corresponding hour. According to these results, there is no loop formed in the microgrid and still tie and sectionalizing switches are changing, often.

As it was mentioned before, a secure energy management framework is considered in this paper within the proposed smart AC-DC hybrid microgrid. In this study, the DC-1, DC-2 and AC microgrids are considered as three different agents of the system underlying the proposed DAG-based security framework and intend to transact their energy and data among themselves. The public transaction is a record holds the public information of the agents and is accessible for a third-party entity. There is a unique transaction blockchain to which the data related to all energy transactions that two different agents have, will be broadcasted and then recorded. On the other hand, each data block in the transaction blockchain holds the data related to two different agents' energy transactions which could be the bilateral energy transactions of AC-to-DC1 or AC-to-DC2. For each one of the parties (DC-1, DC-2, AC), a private blockchain is considered which holds the data related to the units of that party. As previously mentioned, the data blocks form a chain considering the dependency between the HAs of

TABLE 12. Data block framework for AC microgrid at t = 5.

Block1				
Private			Public	Transaction
Previous HA			Previous HA	Previous HA
Aa4bc6ac345470cade6dae9345711112d3			ae5cf9bd356467bfff6dea962341992b2	Ad3bc1ee157269ffce6dfa9376412 81d9
Current HA			Current HA	Current HA
de5bd9ea381469bfcg6dea9631459602a2			126879ea381189bfc11dea96314aebcdf	1e5bf9caaafe69bcda6dea96314596211
MT-2 (KW)	MT-3 (KW)	WT-2 (KW)	Total generation (KW)	AC to DC-1
250	61	25	336	200

a new block and the old one generated in previous hour. For instance, the private blockchain-related to the DC-1 is a record holds the data blocks related to the PV-1, WT-1, FC-1, MT-1 and battery. These power units need to broadcast their information including their price and energy values bidding values. Tables 10, 11 and 12 show the data block structures for DC-1, DC-2 and AC microgrids at $t = 13$, $t = 20$ and $t = 5$, respectively.

VII. CONCLUSION

This paper proposed a secured architecture for the optimal operation of smart hybrid AC-DC microgrids considering different RESs such as WT and PV, high penetration of PEVs, reconfiguration strategy and a detailed model of PEMFC. The proposed framework makes use of a stochastic approach based on MTLA and PEM to solve the optimal power scheduling in the hybrid microgrids, properly. Compared to the Monte Carlo method, the PEM approach is a faster method and the accuracy of which is acceptable for the process. A proper DAG-based data transaction framework is proposed within the smart hybrid AC-DC microgrids in order to enhance the transparency and security of the system. The simulation results on an IEEE test system show the significance of considering thermal power recovery and hydrogen generation in the FC model for supporting part of the thermal demand. Also, it is seen that V2G technology can help for converting the just-consuming role of PEVs into an active role which can store energy at some hours and discharge at later hours, when heavy loaded time. The collaborative power supply of the DC and AC parts of the smart hybrid microgrid provides better power dispatch of units by exchanging power at different hours of the day. From the optimization point of view, the high search ability of the MTLA over GA, PSO and original TLA was demonstrated too. It is also shown that the proposed DAG-based framework is able to effectively enhance the security level of energy and data transactions and diminish the possibility of unauthorized accesses. All things considered, in this work, there has been a secure energy management scheme is provided in which the main agents of the network (DC-1, DC-2, and AC) are able to have effective energy transactions.

It should be noted that WT and PV efficiency and their models are ignored here but will be addressed in the future works.

REFERENCES

[1] *Department of Energy Office of Electricity Delivery and Energy Reliability*, Summary, DOE Microgrid Workshop, Illinois Inst. Technol., Chicago, IL, USA, 2012.

[2] M. Abdelaziz, E. M. Awwad, A. M El-Sherbeeny, E. A. Nasr, and Z. Ali, "Optimal scheduling of reconfigurable grids considering dynamic line rating constraint," *IET Gener., Transmiss. Distrib.*, early access, Feb. 2020, doi: 10.1049/iet-gtd.2019.1570.

[3] A. Nikoobakht, J. Aghaei, T. Niknam, H. Farahmand, and M. Korpås, "Electric vehicle mobility and optimal grid reconfiguration as flexibility tools in wind integrated power systems," *Int. J. Electr. Power Energy Syst.*, vol. 110, pp. 83–94, Sep. 2019.

[4] M. Al-Saud, A. M. Eltamaly, M. A. Mohamed, and A. Kavousi-Fard, "An intelligent data-driven model to secure intravehicle communications based on machine learning," *IEEE Trans. Ind. Electron.*, vol. 67, no. 6, pp. 5112–5119, Jun. 2020.

[5] D. Dallinger, J. Link, and M. Buttner, "Smart grid agent: Plug-in electric vehicle," *IEEE Trans. Sustain. Energy*, vol. 5, no. 3, pp. 710–717, Jul. 2014.

[6] M. Pourbehzadi, T. Niknam, J. Aghaei, G. Mokryani, M. Shafie-khah, and J. P. S. Catalão, "Optimal operation of hybrid AC/DC microgrids under uncertainty of renewable energy resources: A comprehensive review," *Int. J. Electr. Power Energy Syst.*, vol. 109, pp. 139–159, Jul. 2019.

[7] H. Chabok, M. Roustaei, M. Sheikh, and A. Kavousi-Fard, "On the assessment of the impact of a price-maker energy storage unit on the operation of power system: The ISO point of view," *Energy*, vol. 190, Jan. 2020, Art. no. 116224.

[8] M. A. Mohamed, A. S. Al-Sumaiti, M. Krid, E. M. Awwad, and A. Kavousi-Fard, "A reliability-oriented fuzzy stochastic framework in automated distribution grids to allocate μ-PMUs," *IEEE Access*, vol. 7, pp. 33393–33404, 2019.

[9] R. H. Lasseter, "MicroGrids," in *Proc. IEEE Power Eng. Soc. Winter Meeting*, vol. 1. Jan. 2002, pp. 305–308.

[10] A. P. S. Meliopoulos, "Challenges in simulation and design of μGrids," in *Proc. IEEE Power Eng. Soc. Winter Meeting. Conf. Process.*, vol. 1, Jan. 2002, pp. 309–314.

[11] S. Chowdhury, S. P. Chowdhury, and P. Crossley, "Microgrids and active distribution networks," in *Renewable Energy Series*. London, U.K.: IET, 2009.

[12] H. Jiayi, J. Chuanwen, and X. Rong, "A review on distributed energy resources and MicroGrid," *Renew. Sustain. Energy Rev.*, vol. 12, no. 9, pp. 2472–2483, Dec. 2008.

[13] M. A. Mohamed, T. Chen, W. Su, and T. Jin, "Proactive resilience of power systems against natural disasters: A literature review," *IEEE Access*, vol. 7, pp. 163778–163795, 2019.

[14] N. Hatziargyriou, *Microgrids: Architectures and Control*. Hoboken, NJ, USA: Wiley, 2014.

[15] A. Khodaei, "Microgrid optimal scheduling with multi-period islanding constraints," *IEEE Trans. Power Syst.*, vol. 29, no. 3, pp. 1383–1392, May 2014.

[16] M. A. Mohamed, A. M. Eltamaly, A. I. Alolah, and A. Y. Hatata, "A novel framework-based cuckoo search algorithm for sizing and optimization of grid-independent hybrid renewable energy systems," *Int. J. Green Energy*, vol. 16, no. 1, pp. 86–100, Oct. 2018.

[17] C. Chen, S. Duan, T. Cai, B. Liu, and G. Hu, "Smart energy management system for optimal microgrid economic operation," *IET Renew. Power Gener.*, vol. 5, no. 3, pp. 258–267, 2011.

[18] A. G. Tsikalakis and N. D. Hatziargyriou, "Centralized control for optimizing MGs operation," *IEEE Trans. Energy Convers.*, vol. 23, no. 1, pp. 241–248, Mar. 2008.

[19] A. Dukpa, I. Duggal, B. Venkatesh, and L. Chang, "Optimal participation and risk mitigation of wind generators in an electricity market," *IET Renew. Power Gener.*, vol. 4, no. 2, pp. 165–175, 2010.

[20] H. Han, X. Hou, J. Yang, J. Wu, M. Su, and J. M. Guerrero, "Review of power sharing control strategies for islanding operation of AC microgrids," *IEEE Trans. Smart Grid*, vol. 7, no. 1, pp. 200–215, Jan. 2016.

[21] X. Lu, N. Liu, Q. Chen, and J. Zhang, "Multi-objective optimal scheduling of a DC micro-grid consisted of PV system and EV charging station," in *Proc. IEEE Innov. Smart Grid Technol. Asia (ISGT ASIA)*, May 2014, pp. 487–491.

[22] C. Huang, M. Chen, Y. Liao, and C. Lu, "DC MG operation planning Renewable Energy Research and Applications (ICRERA)," in *Proc. Int. Conf.*, Nov. 2012, pp. 1–7.

[23] H. Lotfi and A. Khodaei, "AC versus DC microgrid planning," *IEEE Trans. Smart Grid*, vol. 8, no. 1, pp. 296–304, Jan. 2017.

[24] P. T. Baboli, M. Shahparasti, M. P. Moghaddam, M. R. Haghifam, and M. Mohamadian, "Energy management and operation modelling of hybrid AC-DC MG," *IET Gen. Trans. Dist.*, vol. 8, no. 10, pp. 1700–1711, 2014.

[25] N. Eghtedarpour and E. Farjah, "Power control and management in a hybrid AC/DC MG," *IEEE Trans. Smart Grid*, vol. 5, no. 3, pp. 1494–1505, Apr. 2014.

[26] B. Papari, C. S. Edrington, I. Bhattacharya, and G. Radman, "Effective energy management of hybrid AC–DC microgrids with storage devices," *IEEE Trans. Smart Grid*, vol. 10, no. 1, pp. 193–203, Jan. 2019.

[27] A. Hussain, V.-H. Bui, and H.-M. Kim, "Robust optimal operation of AC/DC hybrid microgrids under market price uncertainties," *IEEE Access*, vol. 6, pp. 2654–2667, 2018.

[28] M. Roustai, M. Rayati, A. Sheikhi, and A. Ranjbar, "A scenario-based optimization of smart energy hub operation in a stochastic environment using conditional-value-at-risk," *Sustain. Cities Soc.*, vol. 39, pp. 309–316, May 2018.

[29] M. Y. El-Sharkh, M. Tanrioven, A. Rahman, and M. S. Alam, "Economics of hydrogen production and utilization strategies for the optimal operation of a grid-parallel PEM fuel cell power plant," *Int. J. Hydrogen Energy*, vol. 35, no. 16, pp. 8804–8814, Aug. 2010.

[30] A. Maleki and M. A. Rosen, "Design of a cost-effective on-grid hybrid wind–hydrogen based CHP system using a modified heuristic approach," *Int. J. Hydrogen Energy*, vol. 42, no. 25, pp. 15973–15989, Jun. 2017.

[31] A. Maleki, "Optimal operation of a grid-connected fuel cell based combined heat and power systems using particle swarm optimisation for residential sector," *Int. J. Ambient Energy*, pp. 1–8, Jan. 2019.

[32] A. Maleki, "Modeling and optimum design of an off-grid PV/WT/FC/diesel hybrid system considering different fuel prices," *Int. J. Low-Carbon Technol.*, vol. 13, no. 2, pp. 140–147, Mar. 2018.

[33] S. Motie, F. Keynia, M. R. Ranjbar, and A. Maleki, "Generation expansion planning by considering energy-efficiency programs in a competitive environment," *Int. J. Electr. Power Energy Syst.*, vol. 80, pp. 109–118, Sep. 2016.

[34] W. Zhang, A. Maleki, and M. A. Rosen, "A heuristic-based approach for optimizing a small independent solar and wind hybrid power scheme incorporating load forecasting," *J. Cleaner Prod.*, vol. 241, Dec. 2019, Art. no. 117920.

[35] A. Kavousi-Fard and T. Niknam, "Optimal distribution feeder reconfiguration for reliability improvement considering uncertainty," *IEEE Trans. Power Del.*, vol. 29, no. 3, pp. 1344–1353, Jun. 2014.

[36] D. Shirmohammadi and H. W. Hong, "Reconfiguration of electric distribution networks for resistive line loss reduction," *IEEE Trans. Power Syst.*, vol. 4, no. 1, pp. 1492–1498, Apr. 1989.

[37] A. Kavousi-Fard, A. Abbasi, T. Niknam, and H. Taherpoor, "Multi-objective probabilistic reconfiguration considering uncertainty and multi-level load model," *IET Sci., Meas. Technol.*, vol. 9, no. 1, pp. 44–55, Jan. 2015.

[38] M. A. Kashem, V. Ganapathy, and G. B. Jasmon, "Network reconfiguration for load balancing in distribution networks," *IEE Proc. Gener., Transmiss. Distrib.*, vol. 146, no. 6, pp. 563–567, Nov. 1999.

[39] M. A. Mohamed and A. M. Eltamaly, *Modeling and Simulation of Smart Grid Integrated with Hybrid Renewable Energy Systems*. New York, NY, USA: Springer, 2018.

[40] H. Nafisi, V. Farahani, M. Abedi, and H. Askarian Abyaneh, "Optimal daily scheduling of reconfiguration based on minimisation of the cost of energy losses and switching operations in microgrids," *IET Gener., Transmiss. Distrib.*, vol. 9, no. 6, pp. 513–522, Apr. 2015.

[41] X. Zhan, T. Xiang, H. Chen, B. Zhou, and Z. Yang, "Vulnerability assessment and reconfiguration of microgrid through search vector artificial physics optimization algorithm," *Int. J. Electr. Power Energy Syst.*, vol. 62, pp. 679–688, Nov. 2014.

[42] E. Dall Anese and G. B. Giannakis, "Risk-constrained microgrid reconfiguration using group sparsity," *IEEE Trans. Sustain. Energy*, vol. 5, no. 4, pp. 1415–1425, Oct. 2014.

[43] Z. Li, S. Bahramirad, A. Paaso, M. Yan, and M. Shahidehpour, "Blockchain for decentralized transactive energy management system in networked microgrids," *Electr. J.*, vol. 32, no. 4, pp. 58–72, May 2019.

[44] K. Biswas and V. Muthukkumarasamy, "Securing smart cities using blockchain technology," in *Proc. IEEE 18th Int. Conf. High Perform. Comput. Commun. IEEE 14th Int. Conf. Smart City, IEEE 2nd Int. Conf. Data Sci. Syst. (HPCC/SmartCity/DSS)*, Dec. 2016, pp. 1392–1393.

[45] P. K. Sharma and J. H. Park, "Blockchain based hybrid network architecture for the smart city," *Future Gener. Comput. Syst.*, vol. 86, pp. 650–655, Sep. 2018.
[46] B. Wang, M. Dabbaghjamanesh, A. Kavousi-Fard, and S. Mehraeen, "Cybersecurity enhancement of power trading within the networked microgrids based on blockchain and directed acyclic graph approach," *IEEE Trans. Ind. Appl.*, vol. 55, no. 6, pp. 7300–7309, Nov. 2019.
[47] G. Verbic and C. A. Canizares, "Probabilistic optimal power flow in electricity markets based on a two-point estimate method," *IEEE Trans. Power Syst.*, vol. 21, no. 4, pp. 1883–1893, Nov. 2006.
[48] R. V. Rao, V. J. Savsani, and D. P. Vakharia, "Teaching-learning-based optimization: A novel method for constrained mechanical design optimization problems," *Comput.-Aided Des.*, vol. 43, pp. 303–315, 2011.
[49] O. Avatefipour, A. S. Al-Sumaiti, A. M. El-Sherbeeny, E. M. Awwad, M. A. Elmeligy, and M. A. Mohamed, "An intelligent secured framework for cyberattack detection in electric vehicles' CAN bus using machine learning," *IEEE Access*, vol. 7, pp. 127580–127592, 2019.
[50] M. Y. El-Sharkh, M. Tanrioven, A. Rahman, and M. S. Alam, "Impact of hydrogen production on optimal economic operation of a grid-parallel PEM fuel cell power plant," *J. Power Sour.*, vol. 153, no. 1, pp. 136–144, Jan. 2006.
[51] J. M. Correa, F. A. Farret, L. N. Canha, and M. G. Simoes, "An electrochemical-based fuel-cell model suitable for electrical engineering automation approach," *IEEE Trans. Ind. Electron.*, vol. 51, no. 5, pp. 1103–1112, Oct. 2004.
[52] C. Wang, X. Yang, Z. Wu, Y. Che, L. Guo, S. Zhang, and Y. Liu, "A highly integrated and reconfigurable microgrid testbed with hybrid distributed energy sources," *IEEE Trans. Smart Grid*, vol. 7, no. 1, pp. 451–459, Jan. 2016.
[53] E. Rosenblueth, "Point estimates for probability moments," *Proc. Nat. Acad. Sci. USA*, vol. 72, no. 10, pp. 3812–3814, Oct. 1975.
[54] H. P. Hong, "An efficient point estimate method for probabilistic analysis," *Rel. Eng. Syst. Saf.*, vol. 59, pp. 261–267, Mar. 1998.
[55] C. Su, "Probabilistic load-flow computation using point estimate method," *IEEE Trans Power Syst.*, vol. 20, no. 4, pp. 1842–1851, Oct. 2005.
[56] M. E. Baran and F. F. Wu, "Network reconfiguration in distribution systems for loss reduction and load balancing," *IEEE Power Eng. Rev.*, vol. 9, no. 4, pp. 101–102, Apr. 1989.

XUAN GONG received the B.Sc. degree from the Anhui University of Technology, in 2006, the M.Sc. degree from the China Lanzhou University of Technology, in 2009, and the Ph.D. degree in electric power system and automation from Wuhan University, in 2013. She is currently working with the School of Electrical Engineering and Automation, Anhui University, Hefei, Anhui, China. Her current research include the operation and control of power systems, new energy power generation technology, electric drive control technology of new energy vehicle, optimization, and smart grids.

FEIFEI DONG received the B.Sc. and Ph.D. degrees in electric power system and automation from Wuhan University, in 2015. She is currently working with the China Electric Power Planning and Engineering Institute, Beijing, China. Her current research interests include the operation and control of power systems, and consultation and review of power transmission and transformation projects.

MOHAMED A. MOHAMED (Member, IEEE) received the B.Sc. and M.Sc. degrees from Minia University, Minia, Egypt, in 2006 and 2010, respectively, and the Ph.D. degree from King Saud University, Riyadh, Saudi Arabia, in 2016. He joined the College of Electrical Engineering and Automation, Fuzhou University, China, as a Postdoctoral Research Fellow, in 2018. He has been a Faculty Member with the Department of Electrical Engineering, College of Engineering, Minia University, since 2008. His current research interests are in the areas of renewable energy, energy management, power electronics, power quality, optimization, smart islands, and smart grids. He has supervised multiple M.Sc. and Ph.D. theses, worked on a number of technical projects, and published various articles and books. He has also joined the editorial board of some scientific journals and the steering committees of many international conferences.

OMER M. ABDALLA received the Ph.D. degree in electrical engineering-electrical machines and instrumentations with the EE Department, Faculty of Engineering, Higher Institute of Mechanical and Electrical Engineering, Sofia, Bulgaria, in 1981. He was appointed as a member of Sudanese and Kuwaiti Engineering Societies, in 1980 and 1985, respectively. He was an Assistant Professor with the Department of Electrical Engineering, Faculty of Engineering and Architecture, University of Khartoum, Sudan, from 1983 to 1985. He was an Associate Professor with the Head of the EE Department, College of Engineering, Sudan University of Science and Technology (SUST), Khartoum, from 1992 to 1996. He was also an Associate Professor with the Dean of the Engineering Faculty, University of Medical Science and Technology (UMST), from 2003 to 2013. He is currently an Associate Professor with the Head of the EE Department, College of Engineering, Prince Sattam bin Abdulaziz University, Saudi Arabia.

ZIAD M. ALI received the B.Sc. and M.Sc. degrees in electrical engineering from the Faculty of Engineering, Assiut University, Assuit, Egypt, in 1998 and 2003, respectively, and the Ph.D. degree from Kazan State Technical University, Kazan, Tatarstan, Russia, in 2010. He worked as a Demonstrator with the Aswan Faculty of Engineering, South Valley University, Aswan, Egypt. He worked as an Assistant Lecturer with the Aswan Faculty of Engineering. He worked as an Assistant Professor, since 2011 till 2016, with the Aswan Faculty of Engineering, Egypt, a Visitor Researcher with the Power System Laboratory, Kazan State Energy University, Russian Federation, from 2012 to 2013, and a Visitor Researcher with the Power System Laboratory, College of Engineering, University of Padova, Italy, from 2013 to 2014. He is currently working as an Associate Professor with the Electrical Department College of Engineering, Wadi Addawasir, Prince Sattam bin Abdulaziz University, Saudi Arabia. His research interest includes power system analysis, FACTS, optimization, renewable energy analysis, smart grids, and material science.